biosensors

MDPI

Article

Rational Design of Oxazolidine-Based Red Fluorescent pH Probe for Simultaneous Imaging Two Subcellular Organelles

Chunfei Wang [1], Hengyi Fu [1], Jingyun Tan [1] and Xuanjun Zhang [1,2,*]

[1] Faculty of Health Sciences, University of Macau, Macau 999078, China
[2] MOE Frontiers Science Centre for Precision Oncology, University of Macau, Macau 999078, China
* Correspondence: xuanjunzhang@um.edu.mo

Abstract: A reversible pH-responsive fluorescent probe, BP, was rationally designed and synthesized, based on protonation and deprotonation gave rise to oxazolidine ring open and close. The fluorescence response of BP against pH ranges from 3.78 to 7.54, which is suitable for labeling intracellular pH-dependent organelles. BP displayed strong red emission at a relatively high pH in living HeLa cells and U87 cells. More importantly, this probe exhibited good colocalization with both mitochondria and lysosomes in these two cell lines, attributing to pH-induced structure tautomerism resulting in an oxazolidine ring open and close that triggered effective targeting of these two organelles. As organelle interactions are critical for cellular processes, this strategy of targeting dual organelles through the structure tautomerism is conducive to further developing more effective and advanced probes for real-time imaging of the interaction between mitochondria and lysosomes.

Keywords: pH-responsive probe; reversible detection; mitochondria and lysosomes; simultaneous colocalization

Citation: Wang, C.; Fu, H.; Tan, J.; Zhang, X. Rational Design of Oxazolidine-Based Red Fluorescent pH Probe for Simultaneous Imaging Two Subcellular Organelles. *Biosensors* **2022**, *12*, 696. https://doi.org/10.3390/bios12090696

Received: 1 August 2022
Accepted: 23 August 2022
Published: 29 August 2022

1. Introduction

Acids and bases exist a dynamic balance in living organisms, whereas pH value effectively reflects the level between acids and bases in cells, body fluids and organs [1]. Intracellular pH ranges from 4.5 in lysosomes to 8.0 in mitochondria [2,3]. Due to the requirement for unique pH values in different regions and organelles, intracellular pH can provide cells with a special circumstance closely related to their physiological activity [3–6]. Moreover, pH plays a decisive role in many biochemical procedures, including metabolism, ion transport, activation of enzymes, and the like [7–11]. Nevertheless, pH abnormalities will disrupt proper cell functions, which is considered a hallmark in some pathophysiological processes, such as inflammation, shock and cancer [12,13]. Consequently, there is tremendous interest in monitoring abnormal pH fluctuations in living cells to understand pathological effects and physiological activities, as well as for the early diagnosis of diseases.

Dynamic organelle interactions regulate intracellular signaling outcomes and it thereby has a close relationship with cell survival [14,15]. Mitophagy, known as the removal of excess and damaged mitochondria [16–18], is a typical paradigm of mitochondria and lysosome interactions. Additionally, mitochondria–lysosome interactions, also involving fusion between mitochondria and lysosomes and mitochondria–lysosome contact (MLC) [19–22], are important intracellular processes in eukaryotic cells. However, dysregulated MLC is also linked to diseases such as Parkinson's disease [23–25]. Fluorescent probes with precise imaging capabilities have been widely used in biological-chemical analyses and have some superiorities in monitoring intracellular and extracellular pH [5,26,27]. Recently, small molecular fluorescent probes have been successfully employed for sensing intracellular pH or pH in different organelles (such as cell nuclei, lysosomes and mitochondria) [28–30]. For acidic lysosomes and alkalescent mitochondria, real-time monitoring by only one fluorescent pH probe can obtain deep insight into the more complicated and important

cellular or subcellular activities, as well as their interactions. Many recent studies have made great success in exploring the contact between lysosomes and mitochondria, as well as a useful biomolecule HClO containing [31–34]. To understand the interactions more fully between mitochondria and lysosomes, fluorescent pH probes can be utilized to simultaneously image them, considering their difference in pH, but there is a lack of powerful tools at present.

Pyridyl nitrogen atoms and phenolic oxygen atoms are frequently utilized as protonated targets in the fluorescent sensing of pH [35,36]. Furthermore, large numbers of supramolecular functional systems have also been implemented to track pH [37]. Currently, a novel fluorescent probe, BP, has been synthesized in terms of pH-dependent equilibria between the ring-opening and ring-closing isomers of oxazolidine. Significantly, the hydroxypropyl group tends to form ring-closed oxazolidine in BP at a relatively high pH, with strong red fluorescence (Scheme 1A). Moreover, BP was also successfully applied for real-time monitoring of pH in living HeLa cells and U87 cells. In particular, BP displayed good colocalization with both mitochondria and lysosomes in these two cell lines, which was attributed to the formation of specific organelle-targeting structures (Scheme 1B). This study provides a new strategy for simultaneously tracking different organelles in real-time cellular visualization. It is anticipated to be rationally applied in further designing more effective probes for the study of organelle interactions, especially mitochondria–lysosome interactions.

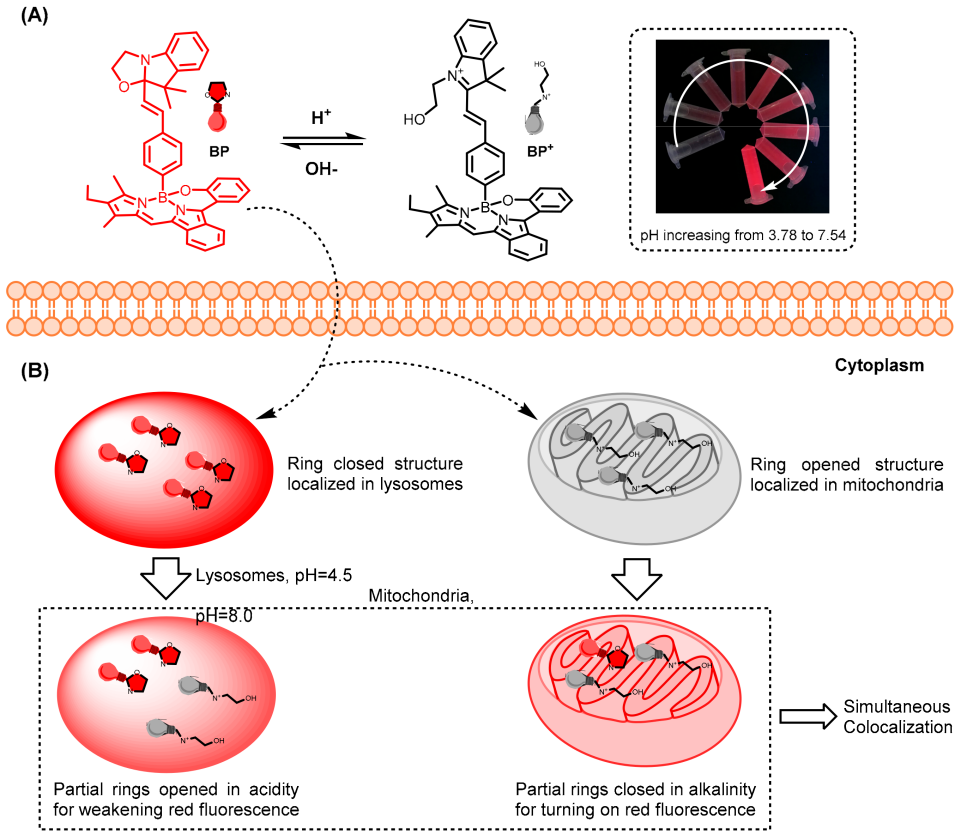

Scheme 1. (**A**) Schematic representation of BP for reversible sensing of pH. (**B**) Simultaneously colocalizing of BP towards mitochondria and lysosomes in living cells.

2. Materials and Methods

2.1. Materials, Instruments and General Methods

Chemicals containing 2,4-dimethyl-3-ethylpyrrole, 2,3,3-trimethyl-3*H*-indole, 2-bromoethanol and other analytes (NaCl, KCl, $CaCl_2$ and $MgSO_4$, ect.) were provided by Dieckman (Hong Kong, China) Chemical Industry Company Ltd. (Hong Kong, China).

Fetal bovine serum (FBS) was purchased from Gibco/BRL (Grand Island, NE, USA). Dulbecco's modified eagle medium (DMEM) and other chemicals (dimethylsulfoxide, DMSO) were obtained from Sigma-Aldrich (St. Louis, MO, USA). MitoTracker Green FM, LysoTracke Green DND-26 and LysoTracker Blue DND-22 were purchased from ThermoFisher (Waltham, MA, USA). All other reagents were AR grade and used without further purification. Distilled water was purified using a Milli-Q water purification system provided by Millipore (Bedford, MA, USA).

NMR spectra detection was recorded by a Bruker AV-400 instrument (Bruker, Karlsruhe, Germany) and reported in ppm downfield. High-resolution mass spectra (HRMS) were obtained by an Xevo G2-XS QTof spectrometer (Waters, Milford, MA, USA). All tested compounds were determined through a reverse phase C_{18} column by peak area integration (Agilent HPLC 1260, Palo Alto, CA, USA). UV/Vis absorption and fluorescent spectroscopy were measured with a UV spectrophotometer (UV-1800, Shimadzu, Kyoto, Japan) and fluorescence spectrophotometer (FluoroMax-4, Horiba, Kyoto, Japan). Cell imaging was evaluated with confocal fluorescence microscopy (Carl Zeiss 710, Jena, Germany).

2.2. Synthesis of pH Probe BP

As described in Scheme 2, BOBPY-CHO was synthesized according to a previous study [38,39]. The synthesis of intermediates **1** and **2** was performed with a previous study for reference [40]. A mixture of 2,3,3-trimethyl-3*H*-indole (20 mmol, 3.06 g) and 2-bromoethanol (25 mmol, 3.12 g) in acetonitrile (20 mL) was refluxed for 24 h under N_2. After cooling to room temperature, the solvent was removed using rotary evaporators. The residue was suspended in hexane (25 mL), sonicated and filtered. The crude solid was recrystallized from chloroform (35 mL) to afford **1** (yield 65.35%). ^{1}H NMR (400 MHz, DMSO) δ = 7.97 (dd, J = 5.6, 3.4, 1H), 7.88−7.83 (m, 1H), 7.65−7.59 (m, 2H), 4.67−4.55 (m, 2H), 3.94−3.82 (m, 2H), 2.83 (s, 3H), 1.55 (s, 6H).

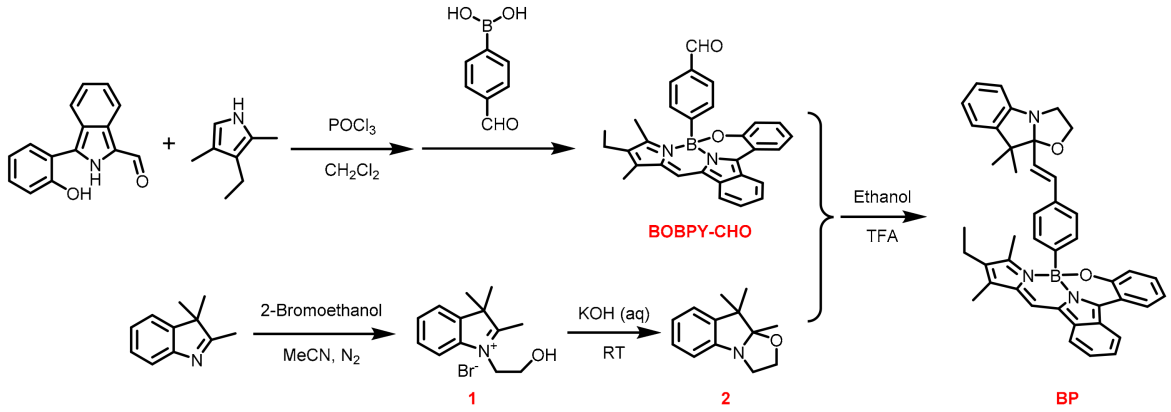

Scheme 2. Synthetic route of different intermediates and BP.

A solution of **1** (10 mmol, 2.83 g) and KOH (15 mmol, 0.84 g) in H_2O (40 mL) was stirred at room temperature for 10 min and then it was extracted with diethyl ether (3 × 20 mL). The organic phase was concentrated under reduced pressure to afford **2** (yield 90.00%) as yellow oil. ^{1}H NMR (400 MHz, Acetone) δ = 7.11−7.05 (m, 2H), 6.84 (td, J = 7.5, 1.0, 1H), 6.77 (dd, J = 8.2, 0.8, 1H), 3.77 (dddd, J = 15.1, 12.0, 7.3, 3.0, 2H), 3.54 (dt, J = 12.0, 8.5, 1H), 3.42−3.35 (m, 1H), 1.37 (s, 3H), 1.32 (s, 3H), 1.13 (d, J = 4.1, 3H). ^{13}C NMR (101 MHz, Acetone) δ = 151.20, 139.91, 127.23, 122.11, 121.08, 111.68, 108.49, 62.55, 49.48, 46.57, 27.35, 20.16, 17.76.

The synthesis of the pH probe, BP, was in accordance with a previous report [41]. Trifluoroacetic acid (TFA, 30 mmol) was added dropwise to a solution of **2** (5 mmol, 1.02 g) and BOBPY-CHO (6 mmol, 2.74 g) in ethanol (10 mL). The mixture was refluxed for 24 h. After cooling to room temperature, the solvent was removed under reduced pressure

and the residue was dissolved in dichloromethane (5 mL). The addition of diethyl ether (200 mL) and refrigeration for 12 h caused the formation of a precipitate. After filtration, the solid residue was dissolved in aqueous $NaHCO_3$ (5% w/v, 20 mL) and stirred for 1 h at ambient temperature. The aqueous mixture was extracted with ethyl acetate (3 × 40 mL). The organic phase was dried over anhydrous Na_2SO_4, filtered and the solvent was distilled off under reduced pressure to give BP (yield 40%). ^{1}H NMR (400 MHz, $CDCl_3$) δ = 8.02 (d, J = 8.3, 1H), 7.90−7.84 (m, 1H), 7.80 (dd, J = 8.1, 0.6, 1H), 7.41−7.34 (m, 1H), 7.31 (d, J = 1.2, 1H), 7.27−7.01 (m, 8H), 6.95 (d, J = 7.0, 1H), 6.88 (t, J = 7.5, 1H), 6.82 (t, J = 7.4, 1H), 6.64 (dd, J = 14.1, 11.9, 2H), 6.03 (dd, J = 15.9, 1.7, 1H), 3.59−3.46 (m, 3H), 3.31−3.19 (m, 1H), 2.40 (d, J = 11.7, 3H), 2.36−2.23 (m, 2H), 2.19 (s, 3H), 1.28 (s, 3H), 1.19 (d, J = 7.0, 3H), 0.98−0.96 (m, 3H). ^{13}C NMR (101 MHz, $CDCl_3$) δ = 157.00, 150.92, 150.66, 150.62, 143.26, 139.79, 139.76, 135.34, 134.38, 133.44, 133.10, 132.84, 132.79, 132.05, 131.93, 130.73, 130.41, 128.77, 127.49, 126.38, 125.46, 124.12, 123.43, 122.35, 120.19, 119.78, 116.01, 109.99, 109.96, 63.40, 63.37, 50.00, 49.94, 47.82, 47.78, 29.72, 29.34, 28.27, 17.49, 14.86, 14.22 13.13, 9.61. HRMS (ESI): calcd. for $C_{43}H_{40}BN_3O_2$ $[M+H]^+$, 642.3292; found 642.3293.

2.3. Preparation of the Test Solution

A stock solution (10 mM) of BP was prepared in DMSO. Then, test solutions of BP were diluted to 2 mL with a mixture of acetonitrile and Britton-Robinson (B-R) buffer solution (v/v = 1:1) with different pH values, which were used to detect UV-vis absorption and fluorescence properties.

The solutions of various analytes were prepared from NaCl, KCl, $CaCl_2$, $MgCl_2$, $FeCl_3$, $CuCl_2$, $ZnCl_2$, $NiCl_2$, $MnCl_2$, $CoCl_2$, $AlCl_3$, arginine, glutamic acid, cysteine, glutathione, H_2O_2 and NaClO, respectively. Small aliquots of each testing species solution were added. The resulting solution was shaken well and incubated for 30 min at room temperature before the fluorescent spectra were recorded.

2.4. Cell Viability Detected by MTT

Human cervical cancer HeLa cells and human glioma U87 cells were cultured in a complete DMEM culture medium containing 10% FBS and 1% penicillin-streptomycin at 37 °C in an atmosphere containing 5% CO_2. After 90% confluence, the cells were cultured in 96-well plates (5000 cells/well, 100 μL). The cells were treated with different concentrations of BP (5, 10, 20, 30, 40, 50, 80 μM) for 24 h. Then, an MTT stock solution (5.0 mg/mL, 100 μL) was added to each well and incubated for 4 h to form a purple crystal formazan. At the end of incubation, DMSO (100 μL) was added, followed by 10 min of microvibration after removing the medium. Absorbance at 570 nm was measured using a microplate reader (Thermo, Waltham, MA, USA).

2.5. Cell Treatment and Imaging

After 90% confluence, HeLa cells and U87 cells were seeded in culture dishes at a density of 1 × 10^5 for 24 h. Before removing the medium, HeLa cells or U87 cells were treated with 10 μM BP for 2 h and washed with PBS buffer (pH = 7.4) three times. Then, HeLa cells and U87 cells were randomly divided into 3 groups and incubated with B-R buffer at different pH values (pH = 3.78, 5.33 and 7.54) for 10 min. After the culture medium was discarded, the cells were fixed. Images were collected by confocal microscopy (Carl Zeiss LSM710, Jena, Germany).

For colocalization of lysosomes and mitochondria, the cells were pretreated with 20 μM MitoTracker Green FM (λ_{ex} = 490 nm and λ_{em} = 513 nm) or 20 μM LysoTracker Green DND-26 (λ_{ex} = 504 nm and λ_{em} = 511 nm) for 30 min and then washed with PBS buffer (pH = 7.4) three times. After that, the cells were treated with 10 μM BP for 1 h. Before imaging, the culture medium was discarded, and the cells were washed with PBS buffer (pH = 7.4) three times and then fixed. Images were also collected by confocal fluorescence microscopy (Carl Zeiss LSM710, Jena, Germany). Data from three independent experiments were then analyzed using Image J.

In addition, the two cell types were pretreated with 20 μM MitoTracker Green FM (λ_{ex} = 490 nm and λ_{em} = 513 nm) and 20 μM LysoTracker Blue DND-22 (λ_{ex} = 373 nm and λ_{em} = 422 nm) for 30 min. After washing with PBS buffer (pH = 7.4) three times, the cells were subsequently incubated with 10 μM BP for 1h. Before imaging, the culture medium was discarded, and the cells were washed with PBS buffer (pH = 7.4) three times and then fixed. Images were also collected by confocal fluorescence microscopy (Carl Zeiss LSM710, Jena, Germany). Data from three independent experiments were then analyzed using Image J.

3. Results and Discussion

3.1. Design and Synthesis of BP

N_2O-type benzopyrromethene boron complexes (BOBPYs) were first developed by Jiao and coworkers [39], wherein different boronic acid derivatives were substituted in the axial position, resulting in high stability, strong absorbance, high fluorescence quantum yields, and narrow emission bands. In addition, N-Hydroxypropyl indole derivatives display oxazolidine ring opening and closing induced by light, temperature and other chemical stimulations (acid-base) [6,40,41]. Nowadays, it has been extensively adopted for pH sensors. BOBPY-CHO, whose axial position was substituted with 4-formylphenylboronic acid, was flexible for further functionalization. Subsequently, the pH probe BP was synthesized by a Knoevenagel reaction with BOBPY-CHO. The detailed synthetic procedures for BP are described in experimental Section 2.2. All products were fully characterized by ^{1}H NMR, ^{13}C NMR and HRMS spectra (Figures S1−S6). Under acidic conditions, a BOBPY-oxazolidine π-conjugated system was displayed, whereas deprotonation triggered oxazolidine ring closing, and π-conjugation was disturbed, resulting in strong red fluorescence in the BP probe.

3.2. Absorption and Fluorescence Response of BP

The absorption and fluorescence spectra of BP were measured in a mixture of MeCN and Britton-Robinson (B-R) buffer solution (v/v = 1:1) with different pH values. As shown in Figure 1A, BP possessed the main absorption peaks at 400 nm and 620 nm. The characteristic absorption peaks at 400 nm decreased with increasing pH from 3.78 to 7.54, which was induced by the opening and closing of the oxazolidine ring. However, the absorption peaks at 620 nm displayed almost no change. BP exhibited a very weak fluorescence peak at 630 nm in the mixture of MeCN and BR buffer solution (v/v = 1:1) when the pH was 3.78, while the peaks increased at pH 7.54, with a 25-fold intensity enhancement (Figure 1B). When the pH was 3.78, the oxazolidine ring opened and iminium ions ($C{=}N^+$) were immediately formed, resulting in fluorescence quenching because of the existence of a BOBPY-oxazolidine π-conjugated system. As the pH increased, BP was more likely to have a closed ring, exhibiting strong red fluorescence due to the destruction of π-conjugated system. Notably, a good linearity (R^2 = 0.9961) between the fluorescence intensity at 630 nm and pH in the range of 3.78 to 5.02 was obtained, as well as in the pH range from 5.33 to 7.54 (R^2 = 0.9321) (Figure 1C,D). Moreover, BP possesses a pKa value of 4.65 related to the oxazolidine switch (Figure S7).

Density functional theory (DFT) calculations were provided to explain the proposed mechanism. As shown in Figure S8 and Table S1, the electrons on the highest occupied orbital (HOMO, −0.1206 eV) and on the lowest unoccupied orbital (LUMO, 0.1584 eV) of BP were all spread in the boron complex part. The electrons on the HOMO of BP^+ were also distributed mainly on the boron complex part, while the electrons on the LUMO of BP^+ located in the axil oxazolidine opening part. Here, we proposed that the quenching of fluorescence in acidic conditions is attributed to the transformation of electrons from the boron complex part to the oxazolidine opening part.

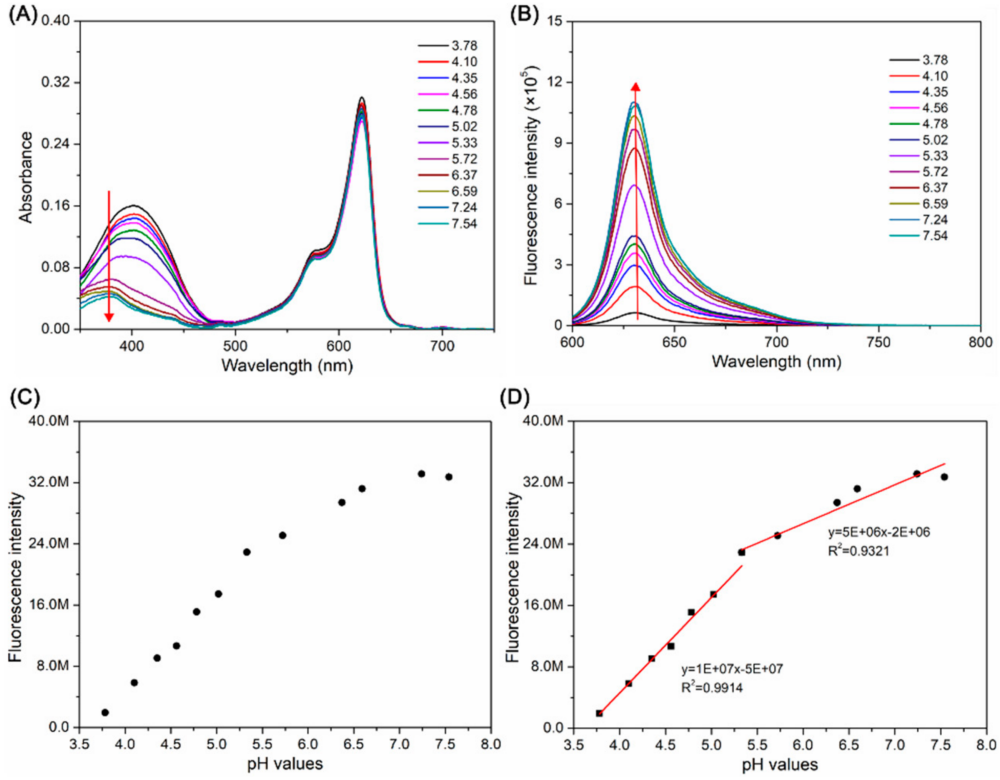

Figure 1. Absorption spectra (**A**) and fluorescent spectra (**B**) of BP (10 μM) in the mixture of MeCN and B-R buffer solution (v/v = 1:1) with different pH from 3.78 to 7.54, excitation: 590 nm. (**C**) Fluorescence intensity of BP (5 μM) at 630 nm in B-R buffer solutions with 50% MeCN at different pH values. (**D**) The linear relationship between the fluorescence intensity of BP (10 μM) at 630 nm and pH values (from 3.78 to 7.54).

3.3. Selectivity Study of BP

To further evaluate the selectivity of BP, we investigated the fluorescence of BP (10 μM) in response to relevant interfering species, including cations, small biomolecules, and reactive oxygen species. As illustrated in Figure 2A, negligible interfering effects on the fluorescence intensity of BP at 630 nm in the presence of all the above species were observed when the pH was 3.78. Additionally, when the pH was 7.54, similar responses were observed, as depicted in Figure 2B. These results demonstrated that the probe possessed excellent selectivity for pH measurement.

3.4. Kinetic and Reversible Studies

The time-dependent fluorescence of BP (10 μM) at pH 3.78 and 7.54 was investigated by recording the fluorescence intensity at 630 nm. As described in Figure 2C, after the addition of BP (10 μM) to B-R buffer solutions with 50% MeCN at pH 3.78 and 7.54, the probe rapidly reached equilibrium and remained relatively stable for at least 4 h. Furthermore, the reversibility of this probe was studied in B-R buffer solutions with 50% MeCN. Particularly, this probe functioned well even after 7 cycles when the pH changed from 3.78 to 7.54 (Figure 2D). Therefore, we believe that this probe can serve as a real-time and reversible monitoring of pH.

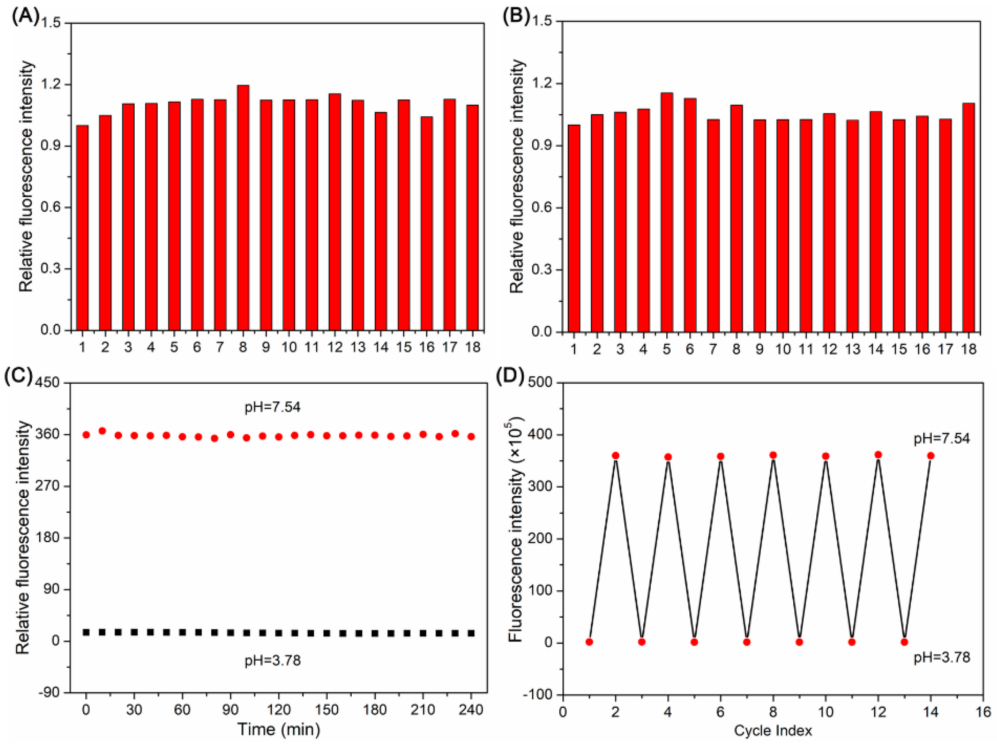

Figure 2. Fluorescence responses of BP (10 μM, 1) at 630 nm in the presence of different metal ions and biologically relevant species at pH were 3.78 (**A**) and 7.54 (**B**). 2. Na^+ (200 μM), 3. K^+ (200 μM), 4. Ca^{2+} (200 μM), 5. Mg^{2+} (50 μM), 6. Ni^{2+} (50 μM), 7. Co^{2+} (50 μM), 8. Mn^{2+} (50 μM), 9. Zn^{2+} (50 μM), 10. Al^{3+} (50 μM), 11. Cu^{2+} (50 μM), 12. Fe^{3+} (50 μM), 13. Cys (50 μM), 14. GSH (50 μM), 15. Glu (50 μM), 16. Arg (50 μM), 17. H_2O_2 (50 μM), 18. ClO^- (50 μM). λ_{ex} = 590 nm. (**C**) The time dependent of the fluorescence intensity of BP (10 μM) in B-R buffer with 50% MeCN at pH was 3.78 and 7.54. (**D**) The fluorescence reversibility of BP (10 μM) in B-R buffer with 50% MeCN between pH = 3.78 and pH = 7.54.

3.5. Cell Imaging with BP at Different pH Values

The aim of this study was to develop an appropriate tool for monitoring pH in biological systems. The MTT study of BP was first assessed in HeLa and U87 cells, which displayed low cytotoxicity at the indicated concentrations, from 5 to 80 μM (Figure S9). To explore the biological application of BP, fluorescent imaging of both HeLa cells and U87 cells was performed at different pH values (3.78, 5.33 and 7.54) in cells treated with 10 μM BP. In Figure 3A, very weak fluorescence was observed in HeLa cells at pH 3.78, whereas significantly enhanced red fluorescence was present in cells treated at pH 5.33 and 7.54. Similar results were also observed in the U87 cells (Figure 3B). The cell imaging results are consistent with the fluorescent properties of BP at different pH values.

3.6. Colocalization of Mitochondria and Lysosomes in Living Cells

In aerobic eukaryotic cells, mitochondria that are energy-producing compartments are central to cell survival and cell death [42,43]. The inner membrane of mitochondria has a proton concentration gradient with a negative charge [44,45]. As a result, small molecules with a positive charge tend to be attracted to the negative potential of the mitochondrial membrane and therefore effectively target mitochondria due to electrostatic attraction [46–48]. We subsequently explored the ability of BP to target and lock in mitochondria. As illustrated in Figure 4, the colocalization experiments with MitoTracker Green FM (λ_{ex} = 490 nm and λ_{em} = 513 nm) demonstrated satisfactory targeting ability, with good Pearson's colocalization coefficients (0.9763 in HeLa cells and 0.8772 in U87

cells). Therefore, BP can localize in mitochondria because it is positively charged in the oxazolidine ring-opening structure.

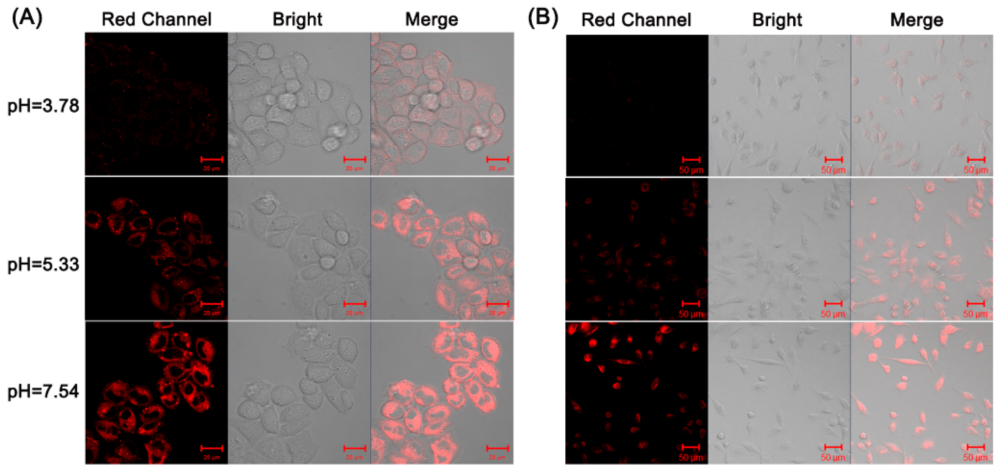

Figure 3. Confocal images of HeLa cells (**A**) and U87 cells (**B**) at different pH levels treated with 10 μM BP. Red channel: λ_{ex} = 561 nm, λ_{em} = 600–750 nm.

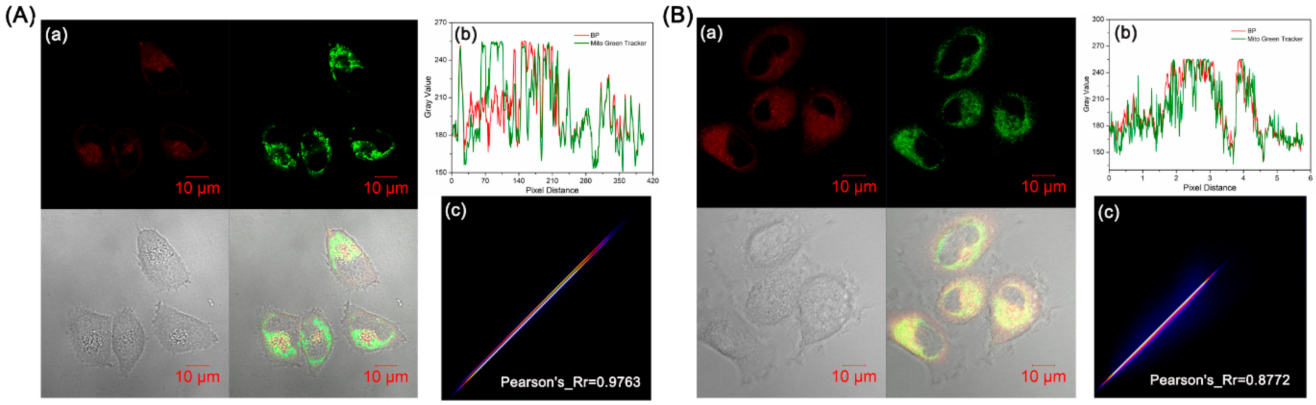

Figure 4. Colocalization experiments of BP and MitoTracker Green FM in HeLa cells (**A**) and U87 cells (**B**). (**a**) Confocal images of cells treated with 10 μM BP, pH = 7.4. (**b**) Plot profile of BP and MitoTracker Green FM. (**c**) Scatter plot of BP and MitoTracker Green FM in cells. Green channel: λ_{ex} = 488 nm, λ_{em} = 490–530 nm; Red channel: λ_{ex} = 561 nm, λ_{em} = 600–750 nm.

Lysosomes, which are membrane-surrounded organelles, play a crucial role in the degradation of almost all content within cells [49–51]. Lysosomes are digestive compartments in cells that exert their activity at low pH [52]. It has been reported that cyclized indolines can localize in lysosomes in a tertiary amine form that acts as a proton receptor [47,53]. This is consistent with the oxazolidine ring-closed structure, which enlightened the colocalization study of BP toward lysosomes. As illustrated in Figure 5, the colocalization experiments with LysoTracke Green DND-26 (λ_{ex} = 504 nm and λ_{em} = 511 nm) also displayed acceptable tracking ability, with Pearson's coefficients of 0.8605 in HeLa cells and 0.7697 in U87 cells. Thus, BP has been reported as a tool for successfully localizing lysosomes. Unexpectedly, BP exhibited the properties of simultaneously tracking mitochondria and lysosomes, which were analyzed as molecular tautomerism with specific organelle-targeting structures induced by pH.

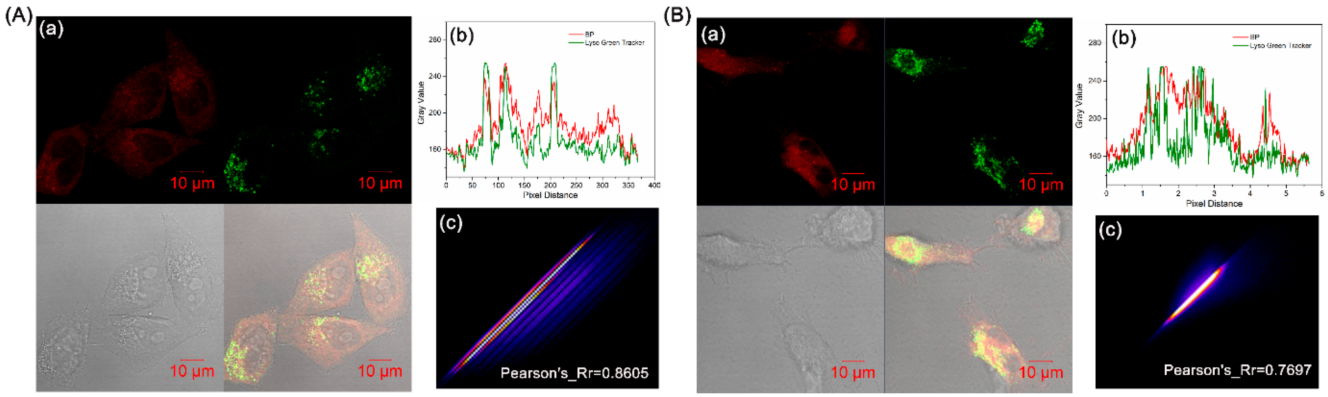

Figure 5. Colocalization experiments of BP and LysoTracker Green DND-26 in HeLa cells (**A**) and U87 cells (**B**). (**a**) Confocal images of cells treated with 10 μM BP, pH = 7.4. (**b**) Plot profile of BP and LysoTracker Green DND-26. (**c**) Scatter plot of BP and LysoTracker Green DND-26 in cells. Green channel: λ_{ex} = 488 nm, λ_{em} = 490–530 nm; Red channel: λ_{ex} = 561 nm, λ_{em} = 600–750 nm.

To better identify the simultaneous colocalization of mitochondria and lysosomes, BP and two organelle-targeting trackers, MitoTracker Green FM (λ_{ex} = 490 nm and λ_{em} = 513 nm) and LysoTracker Blue (λ_{ex} = 373 nm and λ_{em} = 422 nm), were simultaneously adopted for further colocalization experiments [54]. U87 cells and HeLa cells were pretreated with 10 μM BP, subsequently incubated with MitoTracker Green FM and LysoTracker Blue DND-22. As depicted in Figure 6, BP exhibited strong red fluorescence in U87 and HeLa cells (pH = 7.4). Significantly, the overlay between BP and MitoTracker Green (Figure 6A) displayed that the green fluorescence had a desirable overlap with red fluorescence, whereas the non-merged parts (white circle) coincided well with blue fluorescence from LysoTracker Blue. Coincidentally, a similar phenomenon was also observed in HeLa cells (Figure 6B). Additionally, the corresponding Pearson's correlation coefficients were 0.9535 and 0.9069 for mitochondria and lysosomes in U87 cells, while the corresponding Pearson's correlation coefficients were 0.8965 and 0.8487 for mitochondria and lysosomes in HeLa cells. These results more fully proved the simultaneous colocalization of mitochondria and lysosomes by BP.

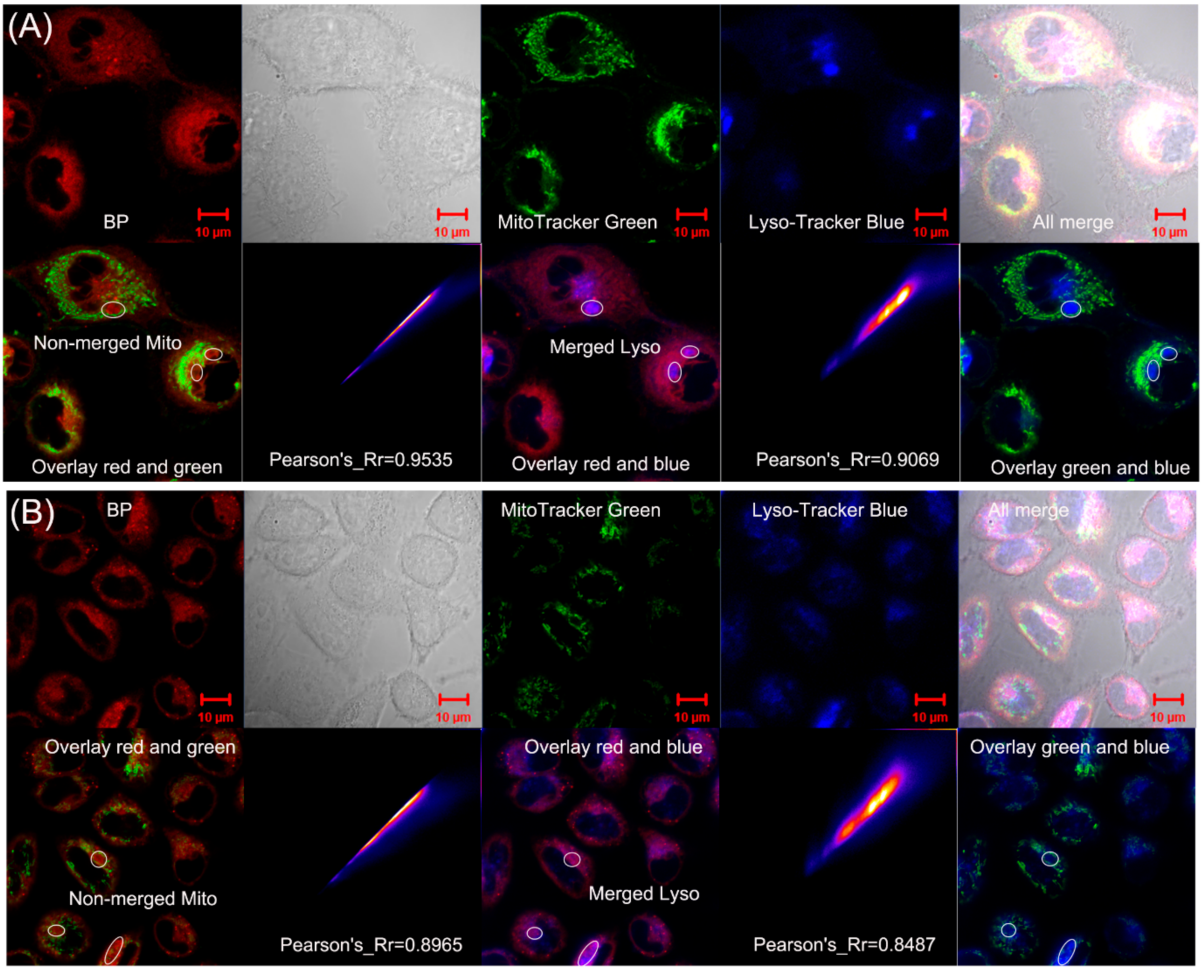

Figure 6. Colocalization experiments of BP with MitoTracker Green FM and LysoTracker Blue DND-22 in U87 cells (**A**) and HeLa cells (**B**). Blue channel: λ_{ex} = 405 nm, λ_{em} = 405–450; Green channel: λ_{ex} = 488 nm, λ_{em} = 490–530 nm; Red channel: λ_{ex} = 561 nm, λ_{em} = 600–750 nm.

4. Conclusions

In the current study, we developed a BOBPY-oxazolidine-derived pH-responsive probe BP for simultaneously imaging mitochondria and lysosomes. The design of BP was based on pH-dependent oxazolidine rings that were open and close. The oxazolidine ring-open structure could convert to a red emissive ring-closed structure in the presence of a relatively high pH. Remarkably, BP exhibited high stability and reversibility, as well as low cytotoxicity, in HeLa cells and U87 cells. It was successfully applied to visualize the pH alterations in both cell lines. Unconventionally, this probe revealed good colocalization with both mitochondria and lysosomes in living HeLa cells and U87 cells, due to pH-induced molecular tautomerism that forms specific organelle-targeting structures. The studied fluorescent pH probe can simultaneously target mitochondria and lysosomes via pH-induced structure tautomerism, which is an advance of fluorescent probes for real-time cellular visualization. Tracking dual organelles with only one fluorescent probe also provides a new strategy for further developing effective fluorescent tools for exploring organelle interactions.

Supplementary Materials: The following supporting information can be downloaded at: https://www.mdpi.com/article/10.3390/bios12090696/s1. Table S1 Calculated excitation energy (eV), oscillator strengths and major contribution for BP and BP^+; Figure S1 ^{1}H NMR spectrum of 1 in DMSO; Figure S2 ^{1}H NMR spectrum of 2 in Acetone; Figure S3 ^{13}C NMR spectrum of 2 in Acetone; Figure S4

^{1}H NMR spectrum of BP in $CDCl_3$; Figure S5 ^{13}C NMR spectrum of BP in $CDCl_3$; Figure S6 HRMS spectrum of BP; Figure S7 Plot curve of fluorescence intensity of 10 μM probe BP versus pH. The information of the curve: Model, Boltzmann. Equation, $y = A2 + (A1 - A2)/(1 + \exp((x - x_0)/dx))$. $pKa = x_0$; Figure S8 Frontier molecular orbital energy diagram of BP and its opening structure BP^+ in a vacuum. Transition energies were calculated using the TD-B3LYP method with 6–31G basis sets; Figure S9 Viabilities of HeLa and U87 cells after incubation with different concentrations of BP for 24 h. Reference [55] are cited in the supplementary materials.

Author Contributions: C.W.: Investigation, Formal analysis, Writing—original draft. H.F.: Methodology. J.T.: Formal analysis. X.Z.: Supervision, Conceptualization, Project administration, Funding acquisition. All authors have read and agreed to the published version of the manuscript.

Funding: This work was funded by the Science and Technology Development Fund, Macau SAR (File No.: 0114/2019/A2, 0085/2020/A2), the Guangdong Basic and Applied Basic Research Foundation (2022A1515010616) and the Research Grant of University of Macau (MYRG2020-00130-FHS).

Institutional Review Board Statement: Not applicable.

Informed Consent Statement: Not applicable.

Data Availability Statement: Not applicable.

Acknowledgments: We also thank the core facilities in the Faculty of Health Sciences, especially the drug development core, animal research core, bioimaging and stem cell core for their excellent services.

Conflicts of Interest: The authors declare no conflict of interest.

References

1. Shartau, R.B.; Baker, D.W.; Crossley, D.A., 2nd; Brauner, C.J. Preferential intracellular pH regulation: Hypotheses and perspectives. *J. Exp. Biol.* **2016**, *219*, 2235–2244. [CrossRef] [PubMed]
2. Smith, F.A.; Raven, J.A. Intracellular PH and its Regulation. *Annu. Rev. Plant Physiol.* **1979**, *30*, 289–311. [CrossRef]
3. Casey, J.R.; Grinstein, S.; Orlowski, J. Sensors and regulators of intracellular pH. *Nat. Rev. Mol. Cell Biol.* **2010**, *11*, 50–61. [CrossRef]
4. Jaworska, A.; Jamieson, L.E.; Malek, K.; Campbell, C.J.; Choo, J.; Chlopicki, S.; Baranska, M. SERS-based monitoring of the intracellular pH in endothelial cells: The influence of the extracellular environment and tumour necrosis factor-alpha. *Analyst* **2015**, *140*, 2321–2329. [CrossRef] [PubMed]
5. Han, J.; Burgess, K. Fluorescent indicators for intracellular pH. *Chem. Rev.* **2010**, *110*, 2709–2728. [CrossRef]
6. Yan, Y.; Fu, H.; Wang, J.; Chen, C.; Wang, Q.; Duan, Y.; Hua, J. A photo-stable and reversible pH-responsive nano-agent based on the NIR phenazine dye for photoacoustic imaging-guided photothermal therapy. *Chem. Commun.* **2019**, *55*, 10940–10943. [CrossRef] [PubMed]
7. Thews, O.; Riemann, A. Tumor pH and metastasis: A malignant process beyond hypoxia. *Cancer Metastasis Rev.* **2019**, *38*, 113–129. [CrossRef]
8. Kim, I.S.; Hwang, M.H.; Jang, N.J.; Hyun, S.H.; Lee, S.T. Effect of low pH on the activity of hydrogen utilizing methanogen in bio-hydrogen process. *Int. J. Hydrog. Energy* **2004**, *29*, 1133–1140. [CrossRef]
9. Deguara, S.; Jauncey, K.; Agius, C. Enzyme activities and pH variations in the digestive tract of gilthead sea bream. *J. Fish Biol.* **2003**, *62*, 1033–1043. [CrossRef]
10. Alfarouk, K.O. Tumor metabolism, cancer cell transporters, and microenvironmental resistance. *J. Enzym. Inhib. Med. Chem.* **2016**, *31*, 859–866. [CrossRef]
11. Hardonniere, K.; Huc, L.; Sergent, O.; Holme, J.A.; Lagadic-Gossmann, D. Environmental carcinogenesis and pH homeostasis: Not only a matter of dysregulated metabolism. *Semin Cancer Biol.* **2017**, *43*, 49–65. [CrossRef] [PubMed]
12. de Valliere, C.; Vidal, S.; Clay, I.; Jurisic, G.; Tcymbarevich, I.; Lang, S.; Ludwig, M.G.; Okoniewski, M.; Eloranta, J.J.; Kullak-Ublick, G.A.; et al. The pH-sensing receptor OGR1 improves barrier function of epithelial cells and inhibits migration in an acidic environment. *Am. J. Physiol. Gastrointest. Liver Physiol.* **2015**, *309*, G475–G490. [CrossRef] [PubMed]
13. Grando, S.A.; Kawashima, K.; Kirkpatrick, C.J.; Kummer, W.; Wessler, I. Recent progress in revealing the biological and medical significance of the non-neuronal cholinergic system. *Int. Immunopharmacol.* **2015**, *29*, 1–7. [CrossRef] [PubMed]
14. Chen, Q.X.; Shao, X.T.; Tian, Z.Q.; Chen, Y.; Mondal, P.; Liu, F.; Wang, F.S.; Ling, P.X.; He, W.J.; Zhang, K.; et al. Nanoscale monitoring of mitochondria and lysosome interactions for drug screening and discovery. *Nano Res.* **2019**, *12*, 1009–1015. [CrossRef]
15. Repnik, U.; Turk, B. Lysosomal-mitochondrial cross-talk during cell death. *Mitochondrion* **2010**, *10*, 662–669. [CrossRef]
16. Kim, I.; Rodriguez-Enriquez, S.; Lemasters, J.J. Selective degradation of mitochondria by mitophagy. *Arch. Biochem. Biophys.* **2007**, *462*, 245–253. [CrossRef]
17. Youle, R.J.; Narendra, D.P. Mechanisms of mitophagy. *Nat. Rev. Mol. Cell Biol.* **2011**, *12*, 9–14. [CrossRef]
18. Tolkovsky, A.M. Mitophagy. *Biochim Biophys. Acta* **2009**, *1793*, 1508–1515. [CrossRef]

19. Lackner, L.L. The Expanding and Unexpected Functions of Mitochondria Contact Sites. *Trends Cell Biol.* **2019**, *29*, 580–590. [CrossRef]
20. Wong, Y.C.; Kim, S.; Peng, W.; Krainc, D. Regulation and Function of Mitochondria-Lysosome Membrane Contact Sites in Cellular Homeostasis. *Trends Cell Biol.* **2019**, *29*, 500–513. [CrossRef]
21. Cohen, S.; Valm, A.M.; Lippincott-Schwartz, J. Interacting organelles. *Curr. Opin. Cell Biol.* **2018**, *53*, 84–91. [CrossRef]
22. Youle, R.J.; van der Bliek, A.M. Mitochondrial fission, fusion, and stress. *Science* **2012**, *337*, 1062–1065. [CrossRef] [PubMed]
23. Burbulla, L.F.; Song, P.; Mazzulli, J.R.; Zampese, E.; Wong, Y.C.; Jeon, S.; Santos, D.P.; Blanz, J.; Obermaier, C.D.; Strojny, C.; et al. Dopamine oxidation mediates mitochondrial and lysosomal dysfunction in Parkinson's disease. *Science* **2017**, *357*, 1255–1261. [CrossRef] [PubMed]
24. Wong, Y.C.; Ysselstein, D.; Krainc, D. Mitochondria-lysosome contacts regulate mitochondrial fission via RAB7 GTP hydrolysis. *Nature* **2018**, *554*, 382–386. [CrossRef] [PubMed]
25. Deus, C.M.; Yambire, K.F.; Oliveira, P.J.; Raimundo, N. Mitochondria-Lysosome Crosstalk: From Physiology to Neurodegeneration. *Trends Mol. Med.* **2020**, *26*, 71–88. [CrossRef]
26. Yue, Y.; Huo, F.; Lee, S.; Yin, C.; Yoon, J. A review: The trend of progress about pH probes in cell application in recent years. *Analyst* **2016**, *142*, 30–41. [CrossRef]
27. Hou, J.T.; Ren, W.X.; Li, K.; Seo, J.; Sharma, A.; Yu, X.Q.; Kim, J.S. Fluorescent bioimaging of pH: From design to applications. *Chem. Soc. Rev.* **2017**, *46*, 2076–2090. [CrossRef]
28. Ge, Y.Q.; Liu, A.K.; Dong, J.; Duan, G.Y.; Cao, X.Q.; Li, F.Y. A simple pH fluorescent probe based on new fluorophore indolizine for imaging of living cells. *Sens. Actuat. B Chem.* **2017**, *247*, 46–52. [CrossRef]
29. Liu, X.; Su, Y.; Tian, H.; Yang, L.; Zhang, H.; Song, X.; Foley, J.W. Ratiometric Fluorescent Probe for Lysosomal pH Measurement and Imaging in Living Cells Using Single-Wavelength Excitation. *Anal. Chem.* **2017**, *89*, 7038–7045. [CrossRef]
30. Nakamura, A.; Tsukiji, S. Ratiometric fluorescence imaging of nuclear pH in living cells using Hoechst-tagged fluorescein. *Bioorg. Med. Chem. Lett.* **2017**, *27*, 3127–3130. [CrossRef]
31. Abeywickrama, C.S.; Baumann, H.J.; Pang, Y. Simultaneous Visualization of Mitochondria and Lysosome by a Single Cyanine Dye: The Impact of the Donor Group (-NR2) Towards Organelle Selectivity. *J. Fluoresc.* **2021**, *31*, 1227–1234. [CrossRef] [PubMed]
32. Yuan, L.; Wang, L.; Agrawalla, B.K.; Park, S.-J.; Zhu, H.; Sivaraman, B.; Peng, J.; Xu, Q.-H.; Chang, Y.-T. Development of Targetable Two-Photon Fluorescent Probes to Image Hypochlorous Acid in Mitochondria and Lysosome in Live Cell and Inflamed Mouse Model. *J. Am. Chem. Soc.* **2015**, *137*, 5930–5938. [CrossRef] [PubMed]
33. Liu, Y.; Zhou, J.; Wang, L.; Hu, X.; Liu, X.; Liu, M.; Cao, Z.; Shangguan, D.; Tan, W. A Cyanine Dye to Probe Mitophagy: Simultaneous Detection of Mitochondria and Autolysosomes in Live Cells. *J. Am. Chem. Soc.* **2016**, *138*, 12368–12374. [CrossRef]
34. Abeywickrama, C.S.; Wijesinghe, K.J.; Stahelin, R.V.; Pang, Y. Bright red-emitting pyrene derivatives with a large Stokes shift for nucleus staining. *Chem. Commun.* **2017**, *53*, 5886–5889. [CrossRef]
35. Park, H.J.; Lim, C.S.; Kim, E.S.; Han, J.H.; Lee, T.H.; Chun, H.J.; Cho, B.R. Measurement of pH Values in Human Tissues by Two-Photon Microscopy. *Angew. Chem. Int. Ed.* **2012**, *51*, 2673–2676. [CrossRef] [PubMed]
36. Jokic, T.; Borisov, S.M.; Saf, R.; Nielsen, D.A.; Kühl, M.; Klimant, I. Highly Photostable Near-Infrared Fluorescent pH Indicators and Sensors Based on BF2-Chelated Tetraarylazadipyrromethene Dyes. *Anal. Chem.* **2012**, *84*, 6723–6730. [CrossRef] [PubMed]
37. Méndez-Ardoy, A.; Reina, J.J.; Montenegro, J. Synthesis and Supramolecular Functional Assemblies of Ratiometric pH Probes. *Chem. A Eur. J.* **2020**, *26*, 7516–7536. [CrossRef]
38. Wang, C.; Cheng, X.; Tan, J.; Ding, Z.; Wang, W.; Yuan, D.; Li, G.; Zhang, H.; Zhang, X. Reductive cleavage of C[double bond, length as m-dash]C bonds as a new strategy for turn-on dual fluorescence in effective sensing of H2S. *Chem. Sci.* **2018**, *9*, 8369–8374. [CrossRef]
39. Chen, N.; Zhang, W.; Chen, S.; Wu, Q.; Yu, C.; Wei, Y.; Xu, Y.; Hao, E.; Jiao, L. Sterically Protected N2O-Type Benzopyrromethene Boron Complexes from Boronic Acids with Intense Red/Near-Infrared Fluorescence. *Org. Lett.* **2017**, *19*, 2026–2029. [CrossRef]
40. Raymo, F.M.; Giordani, S. Signal processing at the molecular level. *J. Am. Chem. Soc.* **2001**, *123*, 4651–4652. [CrossRef]
41. Mazza, M.M.A.; Cardano, F.; Cusido, J.; Baker, J.D.; Giordani, S.; Raymo, F.M. Ratiometric temperature sensing with fluorescent thermochromic switches. *Chem. Commun.* **2019**, *55*, 1112–1115. [CrossRef] [PubMed]
42. Green, D.R. Apoptotic pathways: Ten minutes to dead. *Cell* **2005**, *121*, 671–674. [CrossRef] [PubMed]
43. Newmeyer, D.D.; Ferguson-Miller, S. Mitochondria: Releasing power for life and unleashing the machineries of death. *Cell* **2003**, *112*, 481–490. [CrossRef]
44. Kroemer, G.; Galluzzi, L.; Brenner, C. Mitochondrial Membrane Permeabilization in Cell Death. *Physiol. Rev.* **2007**, *87*, 99–163. [CrossRef] [PubMed]
45. Hoye, A.T.; Davoren, J.E.; Wipf, P.; Fink, M.P.; Kagan, V.E. Targeting Mitochondria. *Acc. Chem. Res.* **2008**, *41*, 87–97. [CrossRef]
46. Zorova, L.D.; Popkov, V.A.; Plotnikov, E.Y.; Silachev, D.N.; Pevzner, I.B.; Jankauskas, S.S.; Babenko, V.A.; Zorov, S.D.; Balakireva, A.V.; Juhaszova, M.; et al. Mitochondrial membrane potential. *Anal. Biochem.* **2018**, *552*, 50–59. [CrossRef]
47. Park, S.J.; Juvekar, V.; Jo, J.H.; Kim, H.M. Combining hydrophilic and hydrophobic environment sensitive dyes to detect a wide range of cellular polarity. *Chem. Sci.* **2020**, *11*, 596–601. [CrossRef]
48. Zhu, H.; Fan, J.; Du, J.; Peng, X. Fluorescent Probes for Sensing and Imaging within Specific Cellular Organelles. *Acc. Chem. Res.* **2016**, *49*, 2115–2126. [CrossRef]
49. Lüllmannrauch, R. *History and Morphology of the Lysosome. Lysosomes*; Springer: Boston, MA, USA, 2005. [CrossRef]

50. de Duve, C. The lysosome turns fifty. *Nat. Cell Biol.* **2005**, *7*, 847–849. [CrossRef]
51. Ciechanover, A. Proteolysis: From the lysosome to ubiquitin and the proteasome. *Nat. Rev. Mol. Cell Biol.* **2005**, *6*, 79–87. [CrossRef]
52. Boya, P.; Kroemer, G. Lysosomal membrane permeabilization in cell death. *Oncogene* **2008**, *27*, 6434–6451. [CrossRef] [PubMed]
53. Chen, W.; Gao, C.; Liu, X.; Liu, F.; Wang, F.; Tang, L.J.; Jiang, J.H. Engineering Organelle-Specific Molecular Viscosimeters Using Aggregation-Induced Emission Luminogens for Live Cell Imaging. *Anal. Chem.* **2018**, *90*, 8736–8741. [CrossRef] [PubMed]
54. Kong, X.Q.; Yin, J.L.; Li, M.; Zhu, L.L.; Dong, B.L.; Ma, Y.Y.; Lin, W.Y. Simultaneously imaging of SO2 in lysosomes and mitochondria based on a dual organelle-targeted fluorescent probe. *Sens. Actuat. B Chem.* **2019**, *292*, 80–87. [CrossRef]
55. Mazi, W.; Yan, Y.; Zhang, Y.; Xia, S.; Wan, S.; Tajiri, M.; Luck, R.L.; Liu, H. A near-infrared fluorescent probe based on a hemicyanine dye with an oxazolidine switch for mitochondrial pH detection. *J.Mater. Chem. B* **2021**, *9*, 857–863. [PubMed]